J Neurophysiol 93: 2039–2052, 2005;
doi:10.1152/jn.00080.2004.

Local Field Potential Oscillations in Primate Cerebellar Cortex: Synchronization With Cerebral Cortex During Active and Passive Expectancy

Richard Courtemanche[1] and Yves Lamarre[2]

[1]*Department of Exercise Science and Center for Studies in Behavioral Neurobiology, Concordia University, Montreal; and* [2]*Département de Physiologie and Centre de Recherche en Sciences Neurologiques, Université de Montréal, Montreal, Canada*

Submitted 26 January 2004; accepted in final form 2 December 2004

Courtemanche, Richard and Yves Lamarre. Local field potential oscillations in primate cerebellar cortex: synchronization with cerebral cortex during active and passive expectancy. *J Neurophysiol* 93: 2039–2052, 2005; doi:10.1152/jn.00080.2004. Many brain regions, such as the cerebellum, primary somatosensory cortex (SI), and primary motor cortex (MI), interact to produce coordinated actions. Synchronization of local field potentials (LFPs) in sensorimotor cerebral areas has been related to motor performance, often through 10- to 25-Hz oscillatory LFPs. The macaque cerebellar paramedian lobule (PM) also shows 10- to 25-Hz LFP oscillations, which are modulated in a stimulus–response lever press task to get reward (active condition), but also, albeit differently, in a similarly timed stimulus–reward relation (passive condition). This study focuses on simultaneous LFP activity in primate SI or MI and the PM cerebellum during the active (left- or right-hand lever presses) and passive conditions. Results show a similar modulation pattern of 10- to 25-Hz oscillations in the cerebellum, MI, and SI during the active condition (left or right hand), decreasing after stimulus onset, returning, and again decreasing after movement onset. In the passive condition, when the monkey did not move but got reward, all 3 areas show an oscillatory profile where oscillations increase after stimulus onset and last until reward, denoting a role for these oscillations in passive expectancy. However, synchronization between cerebellar LFPs and SI LFPs is higher during the active condition than during the passive condition, and highest for the interested hand. This greater PM–SI synchronization, when the monkey had to press the lever, could represent a form of cerebro-cerebellar communication, perhaps to serve somatosensory processing to accomplish the task; PM–MI synchronization was less selective for the hand used and might carry a more general type of information.

INTRODUCTION

Local field potential (LFP) oscillations at 10–40 Hz are present in preparation for movement in monkey parietal and motor cortices (Baker et al. 1997; Donoghue et al. 1998; MacKay and Mendonça 1995; Murthy and Fetz 1996; Rougeul et al. 1979). High-density recordings show that these LFPs represent the collective behavior of neurons surrounding the electrode (Csicsvari et al. 2003), and LFPs can carry a significant amount of information related to motor execution (Mehring et al. 2003; Pesaran et al. 2002). LFP oscillations at 10–25 Hz were also seen in the paramedian lobule (PM) of the cerebellum of the awake monkey (Courtemanche et al. 2002; Pellerin and Lamarre 1997) and at 7–8 Hz (Hartmann and Bower 1998; O'Connor et al. 2002), but also 15–16 Hz (O'Connor et al. 2002) in Crus II of the awake rat. These cerebellar oscillations are specific to the granule cell layer (GCL), when the animal is immobile, and are often stopped by movement (Hartmann and Bower 1998; Pellerin and Lamarre 1997). In the primate cerebellum, PM 10- to 25-Hz LFP oscillations are most prominent when the monkey is attentive and immobile, are closely related to multiunit granule cell firing and also Purkinje cell simple spikes, are modulated during both left- and right-hand lever presses, but are also affected when the monkey is expecting reward without need of movement; these oscillations are thus state-related and differentially modulated during active or passive expectancy (Courtemanche et al. 2002).

Task-related synchronization of LFPs occurs across the primary motor (MI) and primary somatosensory (SI) cortices, before movement for recording sites in MI (Baker et al. 1997) and across MI and SI sites (Murthy and Fetz 1996). Stronger during premovement immobility, β-rhythms in LFPs and electroencephalographic (EEG) data could be involved in attention and readiness (Murthy and Fetz 1996; Pfurtscheller 1981; Rougeul et al. 1979). However, coherence occurs between these β-rhythms and the muscle electromyogram during movement (Baker et al. 1997; Feige et al. 2000; Marsden et al. 2000). This hints at a complex relation between LFPs and movement, in addition to a role in focal attention. Higher frequencies in LFPs could particularly be more sensitive to movement parameters and to particular properties of the cortical area (Pesaran 2003). Roelfsema et al. (1997) reported synchronization of LFP oscillations along the occipito-parietal-motor stream during cat visuomotor behavior, synchronizing even with mildly overlapping frequency bands. Classen et al. (1998) found such large-scale synchronization of EEGs during visuomotor behavior. Movement production possibly even involves the prefrontal cortex for synchronized LFPs in the β-range (Liang et al. 2002); thus synchronization could promote motor binding (König and Engel 1995; MacKay 1997). Interestingly, O'Connor et al. (2002) have shown in the rodent that Crus II cerebellum and SI cortex LFPs share a substantial amount of synchronization (coherence) during pause states, even without movement. Here, we show that PM and SI, and also PM and MI LFP oscillations, are modulated differentially during an active condition when the monkey has to press a lever in response to an auditory stimulus to get reward, compared with a passive condition when the monkey was not required to move but was given reward after a temporal delay after the stimulus. However, more important, the synchroniza-

Address for reprint requests and other correspondence: R. Courtemanche, SP-165-17, Department of Exercise Science, Concordia University, 7141, Sherbrooke Street West, Montreal (Qc) H4B 1R6, Canada (E-mail: rcourt@alcor.concordia.ca).

The costs of publication of this article were defrayed in part by the payment of page charges. The article must therefore be hereby marked "*advertisement*" in accordance with 18 U.S.C. Section 1734 solely to indicate this fact.

tion between cerebellar and cerebral LFPs was also condition-specific, favoring the active condition, and was at its highest for the PM–SI pairs more strongly related to the active hand. Some of these results were presented in abstract form (Courtemanche et al. 1999).

METHODS

Subjects, tasks, and behavior

Tasks and behavior were described fully in a previous report (Courtemanche et al. 2002). Briefly, experiments were conducted on 3 adult *Macaca mulatta* monkeys: 2 males (weights: monkey F, 7.8 kg; monkey Z, 7.0 kg) and one female (monkey K, 4.7 kg). Sitting in a primate chair, they were submitted to 3 conditions: rest, active expectancy, and passive expectancy. Monkey K was recorded only during rest, whereas monkeys F and Z were recorded during rest but were also trained in the active expectancy condition, where they pressed a lever in response to a stimulus after waiting 1,500 ms (sometimes longer for monkey Z), to receive a juice reward. Monkeys F and Z were also tested in the passive expectancy condition, where reward was given without movement, after the same delay. For both conditions, the stimulus was a 400-Hz, 35-dB tone. Lever presses with the left or right hand (active condition left hand or right hand) were rewarded if the monkey pressed the lever between 1,100 and 1,500 ms after the onset of the stimulus. Variants of movement were permitted, provided the lever was pressed within the target window, but through video analysis, movements were stereotypical: monkeys initiated hand displacement toward the lever 250 to 300 ms after stimulus onset, with the movement lasting around 500 ms to reach the lever, and then waited until the end of the delay period to execute the press, which was stored as a voltage change and marked for each trial. For monkey Z, the lever was equipped with a strain gauge for hand contact. Analog video (16.6-ms resolution) was used in some sessions to document the general movement profile. In the passive condition, the lever and supporting table were removed, and the monkey could adopt any posture; however, monkeys remained immobile during the trial, and adopted a sitting posture similar to the one during the active condition.

Each trial lasted 5 s, with intertrial delays varying randomly between 1 and 6 s, for all conditions. Active and passive conditions were presented to the monkey in blocks of trials. In the active condition, instruction for which hand to use was given at the beginning of a block by placing the lever on the left or right of the animal. In the passive condition, the lever was removed, and the monkey only had to sit quietly, but nonetheless received juice after a 1- to 1.5-s delay after stimulus onset. In these blocks, the monkey was still rewarded at the same rate as the active condition (on 60–70% of the trials). Variability in juice delivery time in the passive condition was comparable to the variability in the timing of responses in the active condition.

Recording of local field potentials and movement signals

Recordings were performed simultaneously in the left PM lobule of the cerebellar cortex and the right sensorimotor areas (either SI or MI) of each monkey, with one microelectrode in each (PM–SI or PM–MI arrangements). The center of one recording chamber was positioned over the left posterior parietal/occipital cortex to access the cerebellum, whereas the other was placed over the right central sulcus, using standard methods (Lamarre et al. 1970). Neural activity from the anterior lobe of the cerebellum was recorded a few times during the electrode descent to the PM. Glass-coated tungsten microelectrodes (0.2–0.7 MΩ) captured LFPs (band-pass filtered between 3 and 70 Hz) and unit activity (filtered between 0.3 and 10 kHz), monitored throughout the descent to the targets, which were the top layers of cortex (SI, MI), and the PM lobule GCL. A reference electrode was placed in saline solution (0.9%) above the occipital lobe dura mater in the cerebellar recording chamber. Control recordings for LFP signal reliability were also carried out with a more local reference for cortical recordings in the cerebral cortex chamber saline, or with the reference being the amplifier electrical ground. In these tests, the LFP synchronization was the same as when recorded with the standard supradural occipital reference. Sampling of the LFP signal was at 200 Hz (monkey K) and 1 kHz (monkeys F and Z), whereas lever press and strain gauge signals were sampled at 1 kHz. The LFP signal was also fed on-line to an A/D discriminator for generation of pulse histograms to evaluate signal rhythmicity during the session.

Data analysis and histology

LFPs were analyzed using Fast Fourier Transforms (FFTs) to evaluate rhythmicity, and cross-correlation for synchronization. In the rest condition, we quantified rhythmicity in the 10- to 25-Hz range (Courtemanche et al. 2002; Murthy and Fetz 1996; Rougeul et al. 1979) by calculating the proportion of the signal within these boundaries for consecutive windows, overlapped 50% to better catch oscillation episodes, during which we also calculated the cross-correlation coefficient for synchronization. For a few identified cases, coherence was calculated with the "cohere" algorithm (Matlab, The MathWorks, Natick MA). In the active and passive conditions, rhythmicity during the trial was quantified by computing the temporal spectral evolution (TSE), developed by Salmelin and Hari (1994), and consisting in first band-pass filtering the LFPs (in our case, 10–25 Hz), rectifying this filtered signal, and then averaging this new product across trials. The TSE analysis provides information about the occurrence and amplitude of oscillations at different epochs of the behavioral task. For the synchronization analysis, typically, cross-correlations were performed on 200-ms time windows shifted by 100 ms across the duration of the trial, and peak values of the correlograms for each trial and each time window were averaged for the ensemble of trials and graphed. A control analysis to test the effects of simultaneous rhythmicity, yet separated in time, was performed by cross-correlating the first LFP from the current trial, current window, with the second LFP, previous trial, current window, and so on. This analysis yielded very low values between 0.05 and 0.1, providing importance to the measured interactions in real time (see Figs. 2*D* and 3). For statistical analysis of task-related changes of LFP oscillations and synchronization, testing values were determined by calculating mean values over 3 different epochs: prestimulus (Ps), a 500-ms time window immediately preceding the onset of the stimulus; delay1 (Dl1), a 400-ms window starting 300 ms after stimulus onset; and delay2 (Dl2), a 400-ms time window occurring 400 ms before the lever press, up to the time of the press. For signal rhythmicity and synchronization, respectively, the mean and SDs of the TSE amplitude and the peak cross-correlation coefficient were measured over these 3 windows. For a more accurate view of the modulation of the oscillations, mean TSE during Dl1 and Dl2 was expressed in percentage relative to the mean TSE found during the Ps epoch, set at 0% of change. This allowed pooling of the results of all experiments repeated in the same experimental conditions in the same animal. Multivariate analyses of variance were performed on these relative TSE values and on the cross-correlation values.

In the last recording session, electrolytic lesions were made in the cerebellar and somatosensory cortices of the monkeys at sites where oscillations were found, and 2 days later the monkeys were deeply anesthetized and perfused through the heart using a buffered 9% formaline–8% saline solution. Recording sites were controlled on 50-μm frozen sagittal sections of the cerebellum and cerebrum stained with cresyl violet.

RESULTS

Database

Monkeys K and F were both recorded in the PM–SI and the PM–MI arrangement (K: rest only), and monkey Z was recorded only in the PM–SI arrangement. For the rest condition, 2–10 sessions for each monkey were used to characterize the oscillations and synchronization. The active condition, left hand, was tested in all sessions for monkeys F and Z (3–11 sessions), and the active condition, right hand, was tested for 11 sessions (PM–SI) and 4 sessions (PM–MI) for monkey F. In the passive condition, monkeys F and Z were tested from 3 to 9 sessions. So overall, monkey F was recorded in all task conditions, and was the only one recorded in PM–MI. The histology for monkey F is shown in Fig. 1. For PM GCL recordings, most receptive fields (RFs) elicited were from deep tissue, and needed tapping of the area for the site to be stimulated; most sites (13/14) showed a left arm activation. For SI recordings, almost all RFs were located on the left forearm/wrist area (13/14 sites, one unknown), most often cutaneous (often hair, 8/14). These SI RF properties, along with histological localization of lesions, is consistent with a localization in area 1.

Oscillations in the cerebellum, SI and MI, and synchronization during rest

LFP oscillations in the PM were as described by Pellerin and Lamarre (1997) and Courtemanche et al. (2002), with frequencies between 14 and 21 Hz (mean = 17 Hz). In SI, oscillations were similar to those reported by Rougeul et al. (1979) with frequencies of 16–22 Hz (mean = 18 Hz). Figure 1*A* shows an example of the LFPs simultaneously recorded at a PM site (bottom electrolytic lesion in Fig. 1*C*, indicated by an arrow on the magnified view) and at an SI site (location at lesion site indicated by an arrow in Fig. 1*C*, *top*).

The SI lesion site showed multiunit activity related to cutaneous stimulation of the contralateral forearm and elbow (hair included), and the cytologic organization showed a granular nature, thus corresponding to SI cortex. *Traces* in *A* show that LFPs exhibit waxing and waning episodes of approximately 17-Hz oscillations. For demonstration, FFTs were performed on two 512-ms time periods (gray areas 1 and 2). Part *B* shows that oscillations can center on a precise frequency (epoch 2: 17 Hz), during a time period with strong oscillation at both sites. During epoch 1, when oscillations are less robust, these show a diminished FFT measurement. LFP cross-correlations show that a period of stronger oscillations at both sites (epoch 2) brings a greater synchronization between the LFPs (Fig. 1*D*).

When oscillations were present at the PM site, there was a tendency to have oscillations present at the SI or MI site. This was the case for the most overt type of oscillation (10–25 Hz), in the PM–SI and PM–MI pairs. Figure 2, *A* and *B*, shows the moment-to-moment simultaneous proportion of the LFP signal within 10–25 Hz at each site (cerebellar and cerebral), for experiments in the rest condition of monkey F. There is a clear linear relationship between the 10- and 25-Hz oscillatory content at each site. For both types of comparisons, the corre-

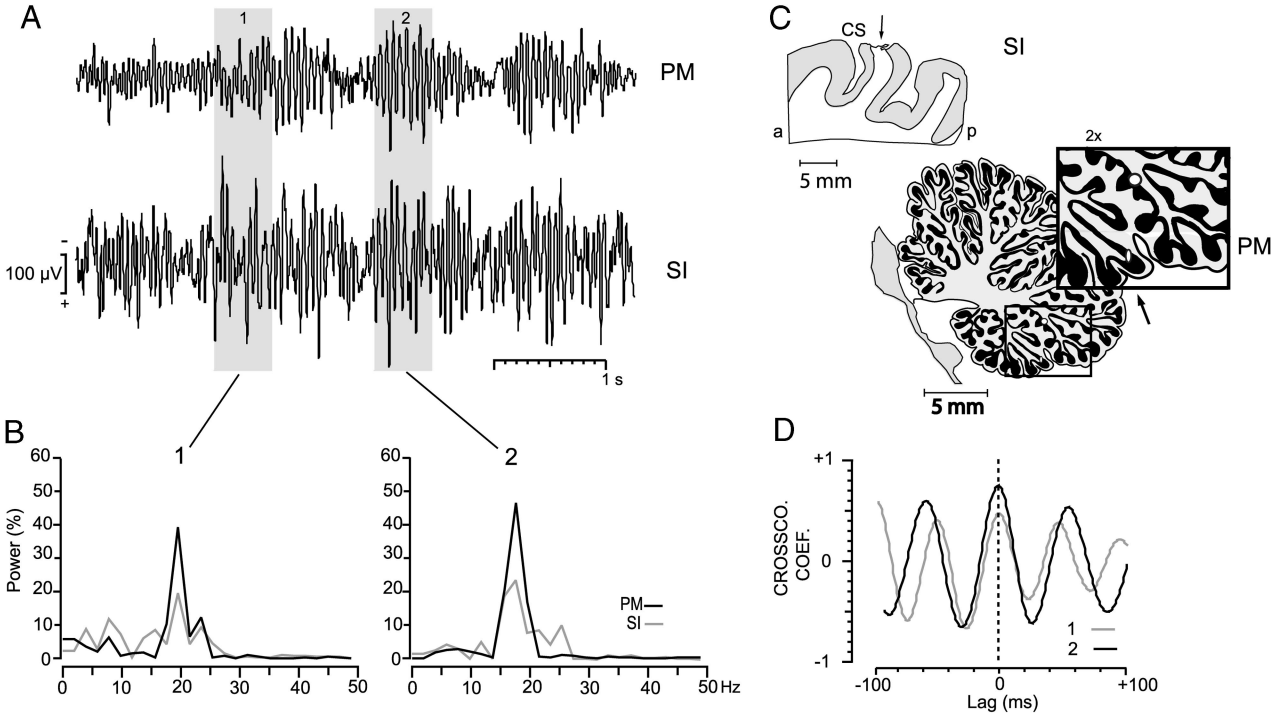

FIG. 1. Local field potential (LFP) oscillations recorded simultaneously in the cerebellum [paramedian lobule (PM)], and the primary somatosensory cortex (SI) of the awake resting monkey F. *A*: *traces* of raw LFP data (sampled at 1,000 Hz). Time periods shaded in gray correspond to time slices of stronger oscillations (period 2), and of weaker oscillations (period 1). *B*: Fast Fourier Transforms (FFT in % of total signal) of the data in *A* (on 512 values), for the periods highlighted by the shading. *C*: location of electrolytic lesion sites in PM and SI before perfusion of the animal, corresponding to sites of 10- to 25-Hz oscillation (arrow pointing to site in SI slice; CS, central sulcus; a, anterior; p, posterior; disturbance of tissue in the posterior lobe of the cerebellum slice, bottom lesion with oscillations). *Inset*: cerebellar slice at a 2 × magnification for greater visibility, arrow pointing to bottom lesion. *D*: cross-correlation coefficient function, for the same highlighted periods (1 and 2) as in *A*, showing higher synchronization, at zero-lag, during period 2.

lation coefficient was almost equivalent ($r = 0.59$ for PM–SI; $r = 0.60$ for PM–MI). The resting condition apparently showed a stable relation between the oscillatory LFPs at the cerebellar and cerebral cortex levels.

Another stable relation occurred for a different type of oscillation, an approximately 30-Hz oscillatory content, in both MI and the anterior lobe cerebellum. These oscillations were localized to a different area of the cerebellar cortex, in the anterior lobe (Courtemanche and Lamarre 1997), but were also of a different type in MI. We found strong correlation between the moment-to-moment 20- to 40-Hz oscillatory content for these sites, as shown in Fig. 2*C* ($r = 0.57$), where monkey K was at rest. This showed the possibility of a stable relation between cerebellar and MI oscillations at more than one frequency band, although our recordings showed a clear spatial and temporal disparity between the approximately 17-Hz and the approximately 30-Hz oscillations at the cerebellar level.

The synchronization of the LFPs, by the peak in the cross-correlogram, was stable throughout the recording period with the monkey at rest. Figure 2*D* shows a peak centered around values around 0.20 (average of all 3 monkeys), whereas the lag was close to 0 ms, but averaged 0, 3, and 6 ms for monkeys K (54 measurements), F (104 measurements), and Z (36 measurements), respectively. As will be shown, these cross-correlation measures were specific to the resting condition. As an indication, coherence measurements showed that LFP synchronization was potent at low frequencies, but mainly interesting here is that an important synchronization component occurred within the 10- to 25-Hz band (PM–SI, Fig. 2*A*, *inset*; PM–MI, Fig. 2*B*, *inset*).

Distribution of the synchronization measures during rest for the PM–SI and PM–MI pairs, for all monkeys, is given in Fig. 3. The cross-correlation coefficient distribution is in Fig. 3, *A* (PM–SI) and *C* (PM–MI), and the corresponding lag is shown in *B* and *D*. Although the number of analysis windows is smaller for the PM–MI pairs because of the smaller sample, cross-correlations were different (both distributions were normal: Kolmogorov–Smirnov test, $P > 0.05$; average cross-correlation was different, PM–SI mean = 0.20 vs. PM–MI = 0.25; $t = -4.15$, $P < 0.0001$), with the values being relatively low for both sets. The lags were also different (the PM–SI distribution was nonnormal: Kolmogorov–Smirnov test, $d = 0.19$, $P < 0.01$; PM–SI mean = 3 ms vs. PM–MI = −3 ms; Wald–Wolfowitz runs test, $z = -6.54$, $P < 0.0001$). The positive lag for the PM–SI pairs means a slight phase advance for the PM site; conversely, the negative lag for the PM–MI pairs means a slight advance for the MI site. At the least, these significant differences show a specificity to the LFPs coming from SI or MI, versus the signal simultaneously recorded in the PM; also they show that the signals collected at the 2 cortical sites were from different sources.

Task-related modulation of PM oscillations and synchronization

These 10- to 25-Hz LFP oscillations from PM and cerebral cortex could become functionally related during task execution: the periods of strongest oscillation were simultaneous during the trials (Fig. 4*B*), and their synchronization was also greatest around the lever press (Fig. 4*C*). LFPs, modulation, and cross-correlation from a single trial in the active condition, left hand, are shown in Fig. 4. Part *A* presents the LFPs recorded simultaneously in PM and SI. The bottom part presents the lever press (L, 1.5 s after the sound onset, S), with FFTs and cross-correlograms corresponding to 4 trial epochs (Ps, Dl1, Dl2, and—added here—Dl3). In addition to rhythm

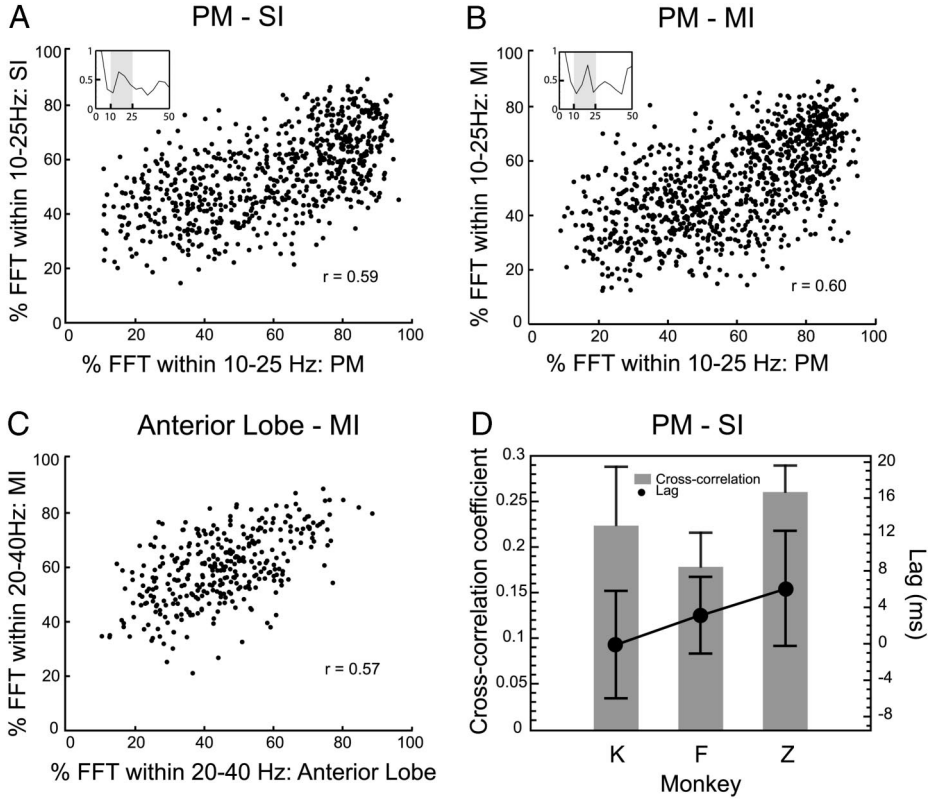

FIG. 2. Simultaneous presence of LFP oscillations in the cerebellum [paramedian lobule (PM) or anterior lobe] and primary sensory (SI) or motor (MI) cortex, along with synchronization, during rest. FFT windows (512-pt) (% of total signal) were moved along the data, with 50% (256-pt) overlap. *A*: degree of correlation of the 10- to 25-Hz content of LFP oscillations in the PM and SI (738 windows), monkey F. *Inset*: average coherence (>4 1-s windows) between PM and SI for the same sites (0- to 50-Hz band shown, gray area 10–25 Hz). *B*: degree of correlation of the 10- to 25-Hz content of LFP oscillations in the PM and MI (990 windows), monkey F. *Inset*: same as in *A*. *C*: degree of correlation of the 20- to 40-Hz content of LFP oscillations in the anterior lobe of the cerebellum and MI (341 windows), monkey K. *D*: cross-correlation values (average and SD) between the LFPs recorded simultaneously in PM and SI in the 3 monkeys (K, F, and Z). Peak amplitude and the lag time of this peak of the cross-correlation coefficient function were evaluated for all windows.

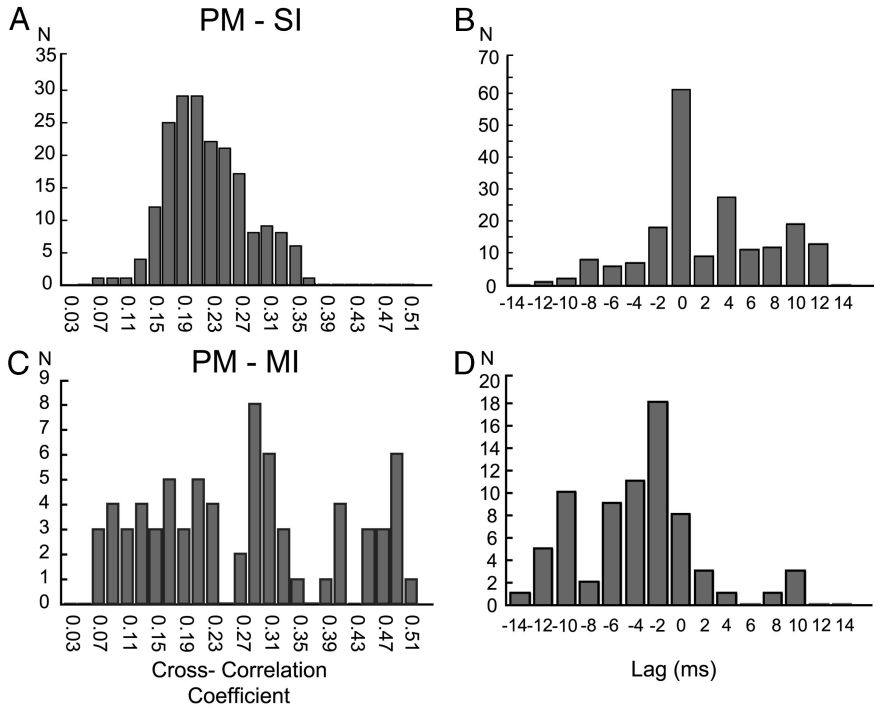

FIG. 3. Synchronization of the PM and SI LFPs, and also of the PM and MI LFPs, during the rest condition, pooled for monkeys K, F, and Z. *A* and *C*: cross-correlation coefficient distribution histogram of PM and SI recording pairs (*A*), and PM and MI recording pairs (*C*). *B* and *D*: corresponding lag distribution histogram. Typical cross-correlation values during the rest condition were around a coefficient of 0.2 yet with a lag around zero, slightly positive for PM–SI, negative for PM–MI (see text).

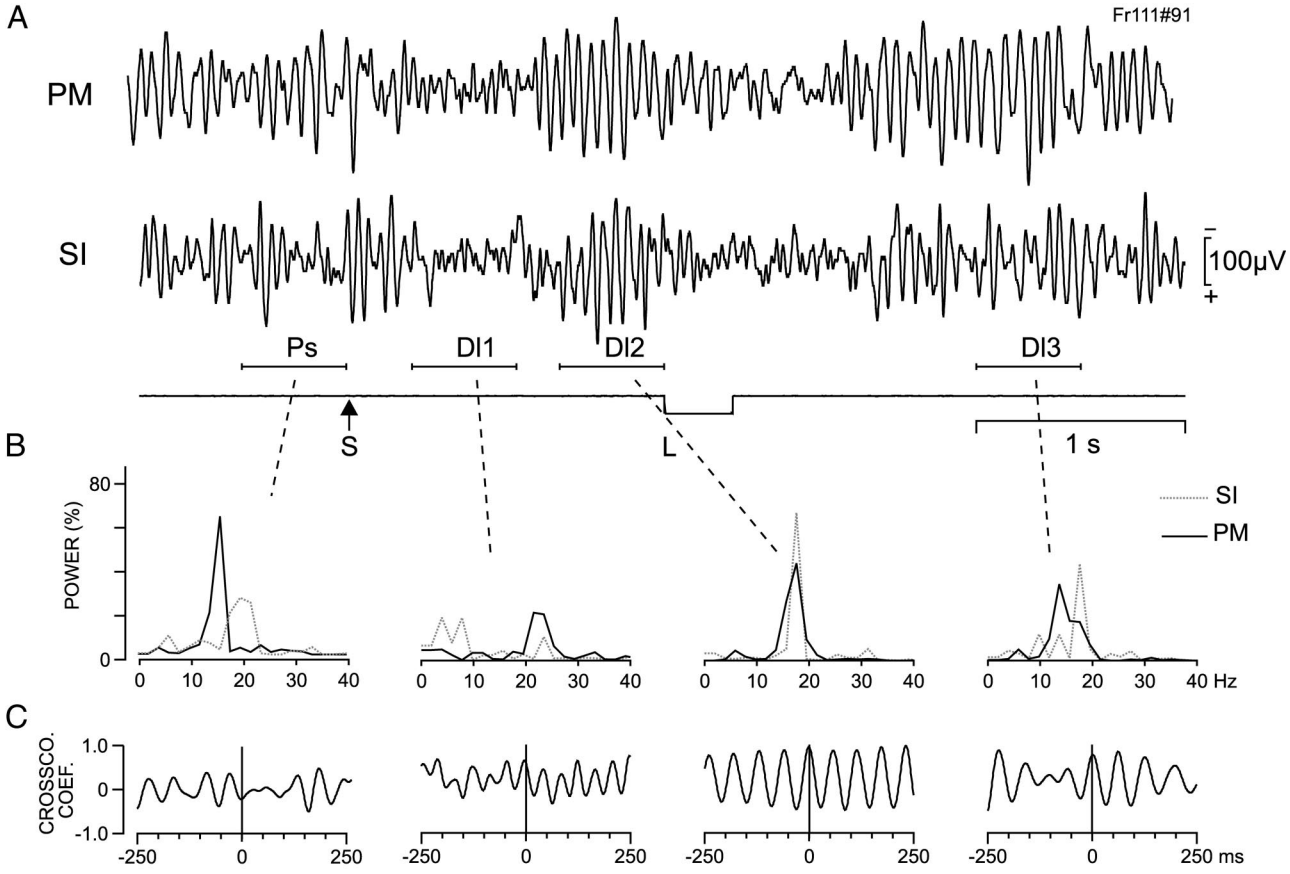

FIG. 4. Modulation and synchronization of PM and SI LFPs during one trial in the active condition left hand. *A*: *LFP traces* recorded simultaneously in the PM and SI, with timeline below showing the appearance of the sound stimulus lasting 1.5 s (S, onset) and the lever press (L, onset). *B*: FFTs (black line, PM; gray line, SI). *C*: cross-correlation coefficient functions corresponding to 250-ms windows at epochs prestimulus (Ps), delay1 (Dl1), delay2 (Dl2), and for display here, delay3 (Dl3). Note the heightened oscillation content at 18 Hz at both sites and increased synchronization during epoch Dl2.

modulation, the consecutive epochs showed different correlations. Oscillations were present in both regions during the Ps epoch, before the appearance of the auditory cue, with respective frequencies at 12–18 Hz for PM and 15–22 Hz for SI. During Dl1, after the appearance of the sound, oscillations were disrupted in both regions. During Dl2, just preceding the lever press, oscillations peaked at 18 Hz in both PM and SI and became highly synchronized with a zero time lag. The oscillations were again disrupted after the lever press and reward delivery but soon resumed (epoch Dl3) with frequencies and correlation similar to epoch Ps. We will first quantify the modulation of oscillations at both LFP sites and then address their synchronization.

Modulation of PM and SI LFP oscillations during active and passive expectancy

Figure 5, *A* and *B*, shows the simultaneously recorded LFPs in the left PM and the right SI during one trial of the active task with the left hand (*A*) or with the right hand (*B*), at the same recording sites. From the raw LFPs, both PM and SI sites show a task-related modulation in oscillations. The 3 epochs (Ps, Dl1, and Dl2) are indicated and, just as was reported in Courtemanche et al. (2002), the PM site showed a stimulus-related decrease in the oscillations during Dl1, an increase before the press during Dl2, and then another, movement-related, decrease after the lever press, a stereotypical modulation pattern. New data presented here show that the modulation pattern was similar for SI LFP oscillations. Below the LFPs, the lever press occurred 1.4 s after the sound onset for the left hand (Fig. 5*A*) and 1.1 s for the right hand (Fig. 5*B*). Figure 4, *C* (left hand: 59 trials) and *D* (right hand: 46 trials), shows the amount of 10- to 25-Hz oscillation in the correct trials for the whole experiment. The average TSE is overlaid for the PM (black line) and SI (gray line), and at the bottom is shown the superimposed lever contact traces for all the trials. The decrease during Dl1, the return to higher values during Dl2, and the decrease afterward are obvious from the TSE traces: the magnitude of these changes were greater for the left hand than for the right hand. In Fig. 5, *E* and *F*, modulation from 9 experiments when both the left and right hand were tested is presented. The average TSE values for the Ps, Dl1, and Dl2 periods were calculated for the correct trials in a session, and evaluated relative to the Ps value, normalized at 0%, providing a normalized TSE value relative to the Ps period. In Fig. 5, *E* (active task, left hand) and *F* (active task, right hand), on the *left* are the PM values and on the *right* are the SI values. During the Dl1 period, the TSE tended to be lower than the Ps level, for all 9 experiments with the left hand, both for PM and SI. For the right hand, there were 8/9 experiments that showed lower TSE values during Dl1 than during the Ps period for both

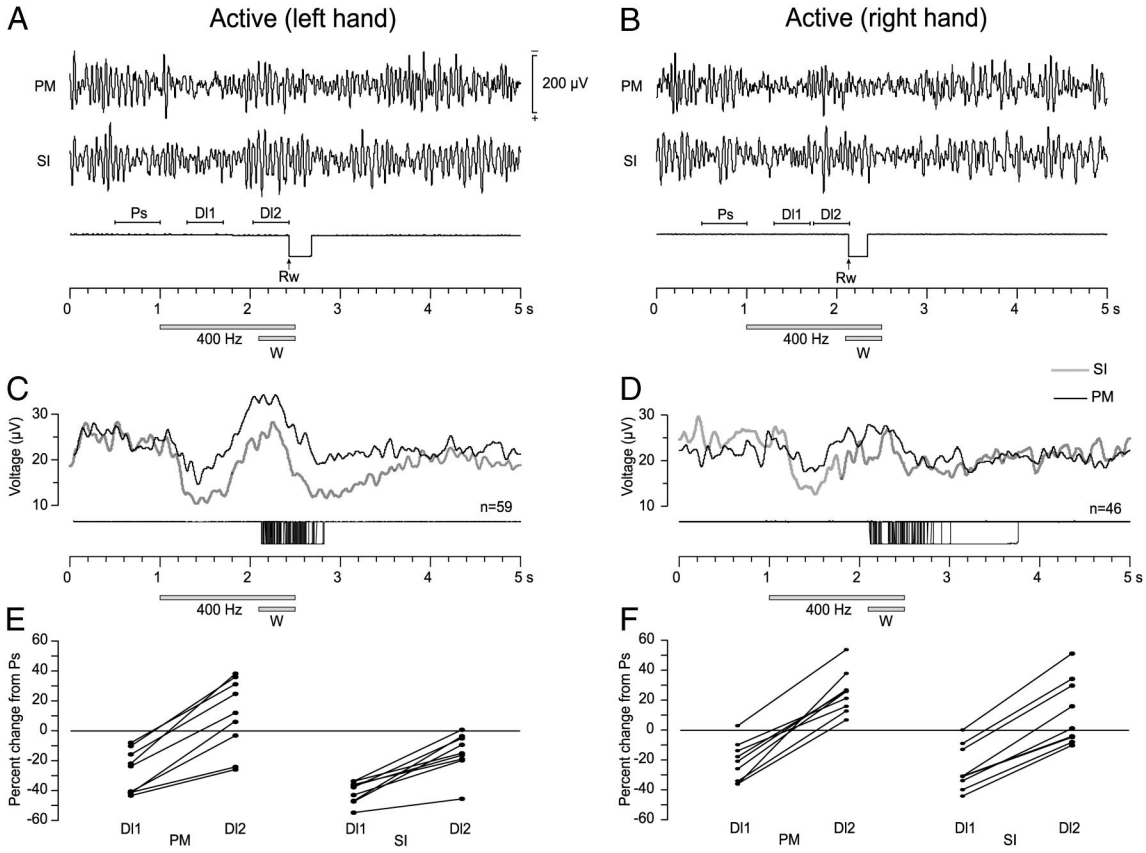

FIG. 5. Modulation of LFP 10- to 25-Hz oscillations in the PM and SI during one session, active condition (left hand on *left side A*, *C*, *E*; right hand on *right side B*, *D*, *F*) for monkey F. *A* and *B*: *LFP traces* recorded simultaneously in the PM and SI during one trial. Lever press time course for this trial is indicated below (Rw, reward delivery). *C* and *D*: temporal spectral evolution (TSE) values collected in the PM and SI over one experiment, rewarded trials. Average PM TSE in black, SI in gray. Lever presses for the whole experiment are overlaid below. Sound stimulus window, 400 Hz; reward window, W, indicated, and number of trials indicated. Delays Ps, Dl1, and Dl2 also illustrated. *E* and *F*: TSE modulation over a series of experiments ($n = 9$) when both the left and right hands were tested, for the PM and SI LFPs. TSE values were calculated for delays Ps, Dl1, and Dl2, and made relative to the Ps for each experiment, fixed at 0%.

PM and SI. Also, there was a return of the oscillatory content during Dl2, for all experiments in Fig. 5*E* (6/9 experiments showing higher values than during the Ps period) for PM and all experiments (although with only 1/9 reaching Ps levels) for SI with the left-hand active condition. In the right-hand active condition, 8/9 experiments showed a decrease in the TSE during the Dl1 period, for PM and SI. The Dl2 period showed a return of the oscillations for PM and SI, all surpassing the Ps levels for PM, and 5/9 for SI. A stable pattern of modulation emerged across experiments for the active condition, whether performed by the left or right hand. This modulation pattern was more pronounced for the left hand (ipsilateral to PM site and contralateral to the SI site), but also could apply to the right hand.

This stable modulation pattern for PM and SI during the active condition is compared with the passive condition in Fig. 6. A single trial from a recording pair with both the active and passive conditions is shown in Fig. 6, *A* and *B*. In the active condition with the left hand (Fig. 6*A*), LFPs for PM and SI show the same modulation pattern as that in Fig. 5*A*, whereas the passive condition (Fig. 6*B*) exhibits a different modulation pattern for both PM and MI, with no decrease after stimulus onset (Dl1), but an increase in oscillations from the beginning of the sound up to the end of the stimulus–reward delay (encompassing both Dl1 and Dl2). The modulation patterns for the same PM and SI pairs also differ in Fig. 6, *C* (active, left hand) and *D* (passive). TSE patterns in Fig. 6*C* reflect the active condition (similar to Fig. 5), but in Fig. 6*D*, the TSE increased for both PM and SI during the stimulus–reward delay in the passive condition, a dramatic increase for the PM site. Relative differences from Ps values during Dl1 and Dl2 for all 9 experiments, when both the left-hand active condition and the passive condition were tested, are shown in Fig. 6, *E* and *F*. The TSE decrease during Dl1 and return of the LFP oscillations during Dl2 in PM and SI are clear for the left-hand condition (*E*), but are very different in *F*, where all but one experiment show an increase in the PM TSE during Dl1, and all but 2 experiments show an increase in the SI TSE during Dl1. The increase goes to much higher values for both PM and SI for all experiments during Dl2. For the PM LFPs, there is thus a contrast in 10- to 25-Hz oscillations between the active and passive conditions (as shown in Courtemanche et al. 2002), and here this contrast is also valid for SI 10- to 25-Hz LFP oscillations.

The raw TSE for all experiments ($n = 10$) in monkey F were submitted to a condition (3: active left hand, active right hand, passive) × recording site (2: PM lobule and SI cortex) × delay (3: Ps, Dl1, and Dl2) MANOVA with repeated measures on the delay factor. The analysis yielded main effects of condition [$F(2,54) = 5.79$, $P < 0.01$], recording site [$F(1,54) = 9.42$, $P < 0.01$], and delay [$F(2,108) = 76.23$, $P < 0.0001$]. A significant interaction was found between condition and delay [$F(4,108) = 15.47$, $P < 0.0001$]. The delay showing the greatest oscillation content was Dl2, the period preceding the lever press and/or reward delivery. The condition × delay

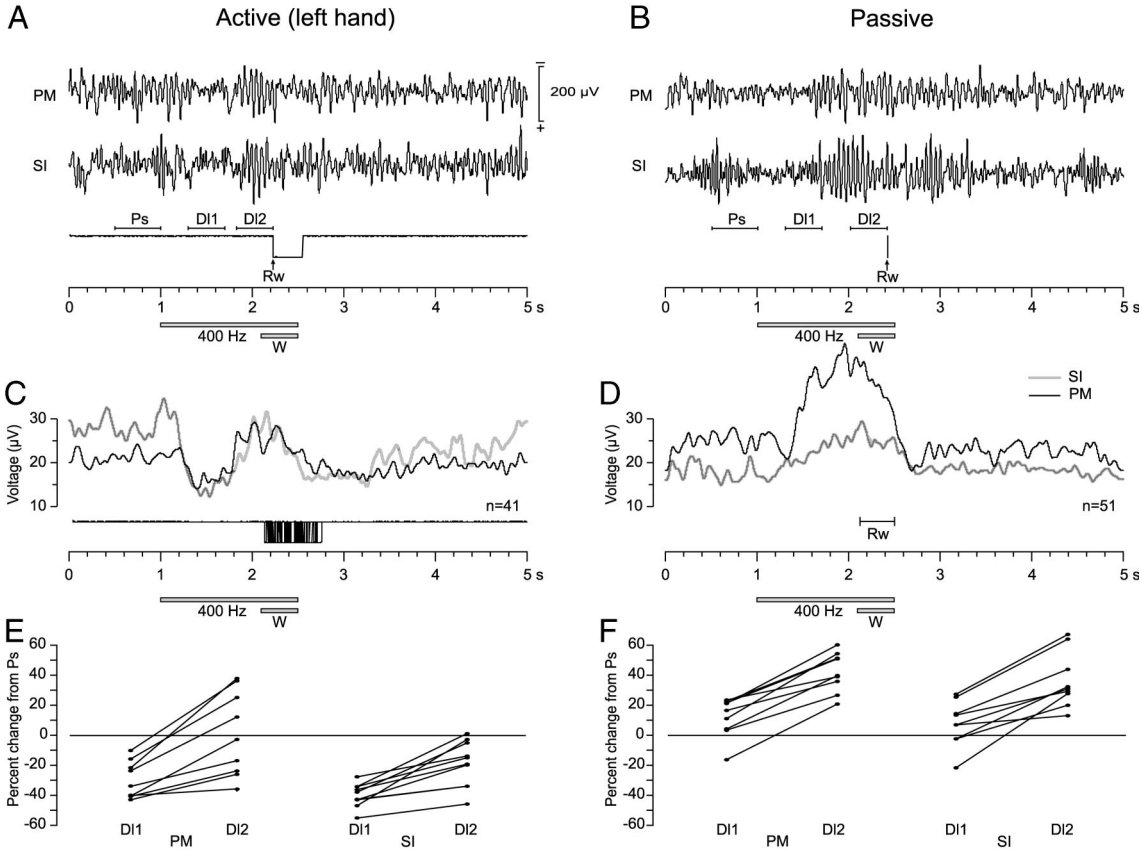

FIG. 6. Modulation of LFP 10- to 25-Hz oscillations in the PM and SI during the active condition (left hand) and passive condition. Data for one trial (*A* and *B*), one session (*C* and *D*), and 9 sessions when both conditions were tested (*E* and *F*), active condition and passive conditions (active condition left hand on *left side A*, *C*, *E*; passive condition on *right side B*, *D*, *F*) for monkey F. Organization of each panel same as in Fig. 4.

interaction showed that the active and passive conditions were different in terms of TSE content over time.

For the relative TSE modulation, regardless of variations in rhythmicity at a site during the Ps period, we also performed a similar condition (3: same as above) × recording site (2: same as above) × delay (2: Dl1 and Dl2) MANOVA with the delay as repeated measures on TSE data relative to the Ps values. For monkey F, as for the raw TSE values, main effects of condition [$F(2,54) = 40.54$, $P < 0.0001$], site [$F(1,54) = 7.00$, $P < 0.05$], and delay [$F(1,54) = 343.98$, $P < 0.0001$] were found on the relative TSEs. The condition × delay interaction was also significant [$F(2,54) = 3.67$, $P < 0.05$], as was the recording site × delay interaction [$F(1,54) = 6.29$, $P < 0.05$]. For the main effect of condition, the passive condition was the least effective at decreasing the TSE, the most being the left-hand active condition, with the right-hand active condition falling in between. The main effect of delay showed that the task affected the TSE during both Dl1 and Dl2 delays. The condition × delay interaction showed that the passive condition permitted a TSE increase during Dl1 and Dl2. The relative TSE values by condition, site, and delay are represented in Fig. 7, with the Ps TSE value fixed at 0% change. Monkey Z was not recorded in the right-hand active condition, but nevertheless the 2 × 2 × 2 MANOVA on the 3 experimental sessions showed main effects of condition [$F(1,8) = 14.94$, $P < 0.005$] and delay [$F(1,8) = 31.01$, $P < 0.001$]. In this monkey, the passive condition TSE was also less decreased during Dl1 and Dl2 (showing increases during Dl2), supporting the active–passive condition differences from monkey F.

Synchronization of PM and SI LFPs during active and passive expectancy

Figure 8 illustrates the PM–SI cross-correlation averaged over one active condition session for monkey F, calculated over 200-ms windows shifted 100 ms to cover the trial. In Fig. 8*A* (left hand: 103 trials), PM and SI LFPs became more synchronized during Dl2 (filled circles). A control condition for fortuitous synchronization (gray line) was evaluated from the LFPs of the same session and sites, as the monkey was sitting quietly (41 "trials," during which no stimulus was given). Figure 8*A* shows that the left-hand active condition promoted increased PM–SI cross-correlations near the lever press.

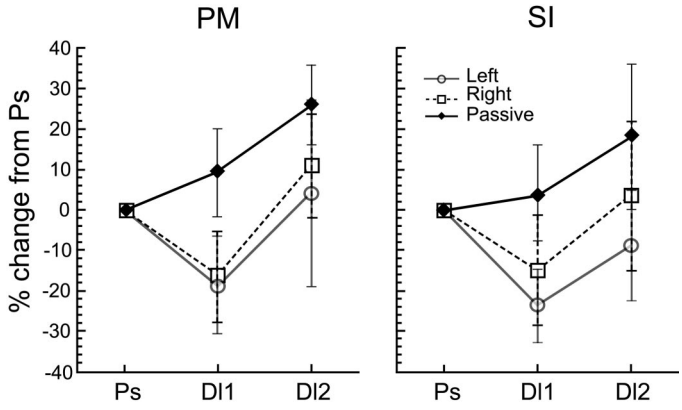

FIG. 7. Modulation of the LFP 10- to 25-Hz oscillatory content during the active and passive conditions, for the PM and SI sites, for the 3 delays, Ps, Dl1, and Dl2. TSE values have been normalized relative to the Ps delay, fixed at % change. Average ± 1SD of the relative TSE values for each condition (active left hand: open circles; active right hand: open squares; passive: filled diamonds) for the 10 experiments in monkey F are shown.

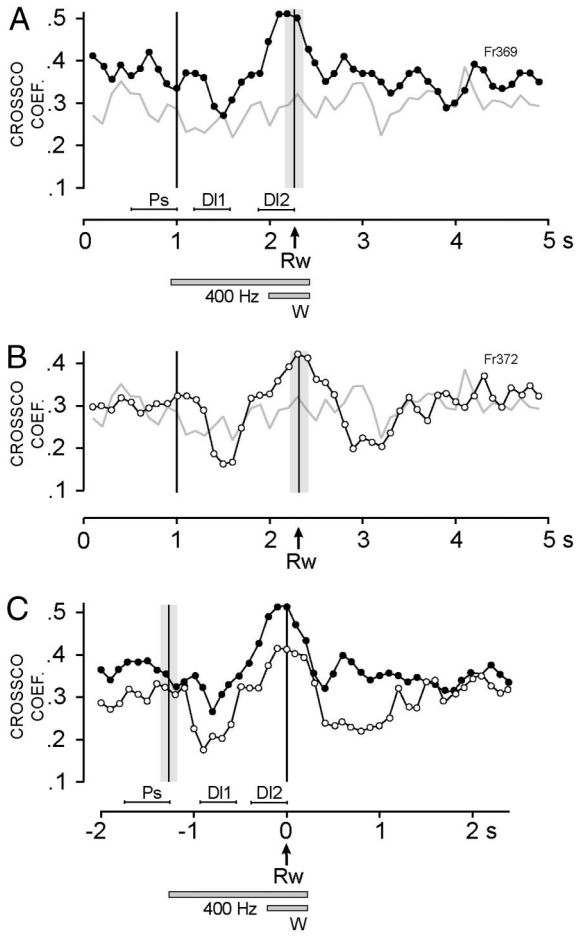

FIG. 8. Synchronization between the PM and SI LFPs in the active condition for one session in monkey F. *A*: averaged cross-correlation coefficients between PM and SI LFPs in the active condition left hand (103 trials, filled circles) and the same while the monkey was just sitting quietly in the chair (control, 41 trials, gray line). *B*: same as in *A* in the active condition right hand (75 trials, open circles). *C*: comparison between cross-correlation coefficients in the active left (filled circles) and right (open circles) hand conditions, same data as in *A* and *B*. *A* and *B* are aligned on the beginning of the trial, *C* is aligned on the lever press onset. Cross-correlation coefficient functions were calculated for successive 200-ms windows shifted by 100 ms. Vertical lines with shaded areas: mean and SD. Ps, prestimulus; Dl1, delay 1; Dl2, delay 2 are indicated. Sound stimulus, 400 Hz; reward window, W; Rw, average time of reward delivery (lever press onset).

PM and SI synchronization could occur with right-hand responses (75 trials; Fig. 8*B*, same recording session as in *A*). However, the synchronization increase around the lever press was not as potent as with the left hand, but different from control, which was essentially flat. Figure 8*C* shows that the cross-correlation coefficient increases for the same trials as in *A* (filled circles) and *B* (open circles) were aligned on the lever press.

The task parameter leading to increased synchronization was still to be determined. For monkey Z, the lever was equipped with a strain gauge for measuring force application. This added information indicated that the increased synchronization during movement was related to the force profile when pressing the lever. Figure 9 displays in *A* the PM–SI cross-correlation

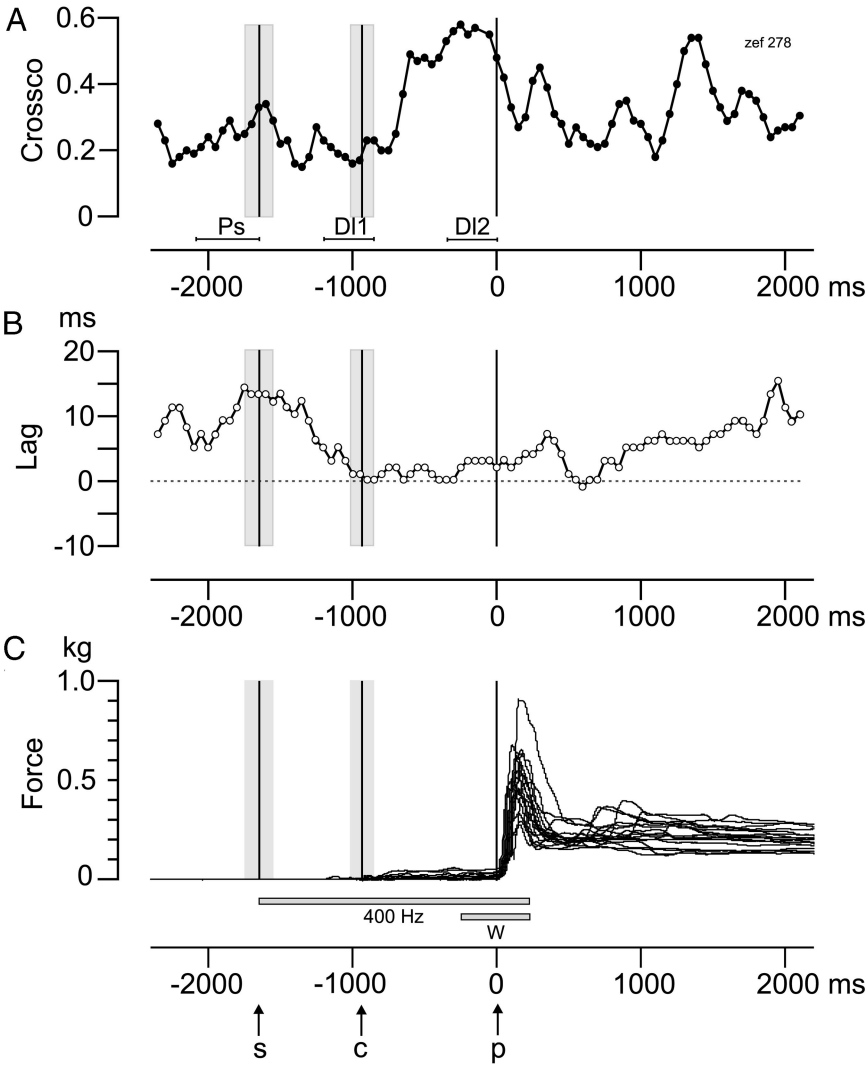

FIG. 9. Specific relation between task parameters and synchronization between the PM and SI LFPs, active condition left hand for one session in monkey Z. Cross-correlations calculated relative to the lever press, on successive 100-ms windows shifted by 50 ms. *A*: cross-correlation coefficient. *B*: corresponding lag. *C*: force applied on the strain gauge connected to the lever. Vertical lines with shaded areas, mean and SD; s, stimulus onset; c, contact of hand to the lever; p, press of the lever. This experiment had a stimulus-ON (400 Hz) time of 1.8 s, and a reward window (*W*) of 500 ms. Time of highest synchronization corresponds to the period of time when the hand was touching the lever, stationary, before the press.

across the trial, aligned on the onset of the lever press; in *B*, the cross-correlation lag; and in *C*, the force measurement, for one session (19 trials) of active task with the left hand. The cross-correlation coefficients increased during the time just preceding the lever press (Dl2), whereas the lag decreased toward zero, attained as the cross-correlation peaked (slightly longer than Dl2, around −600 to 0 ms). Trials were selected for longer delays, when cross-correlation coefficients showed a "plateau," providing additional information to the synchronization curves in Fig. 8. Considering the force profile (part *C*), in a typical trial, the animal rested the hand on the lever just before the phasic movement to depress the lever: the highest cross-correlation coefficient and the smallest lag occurred during this pause. The highest cross-correlation coefficients corresponded to the return of PM oscillations before movement, and lasted until just before the time of the press. This shows a stereotypical pattern of synchronization in active expectancy, as a task-related movement pause served possibly to synchronize PM and SI LFPs before movement. Tactile processing could be a component guiding this synchronization.

Figure 10 shows the 3-delay representation of the LFP cross-correlation coefficients for the 10 sessions and 3 conditions in monkey F. A condition (3: active left hand, active right

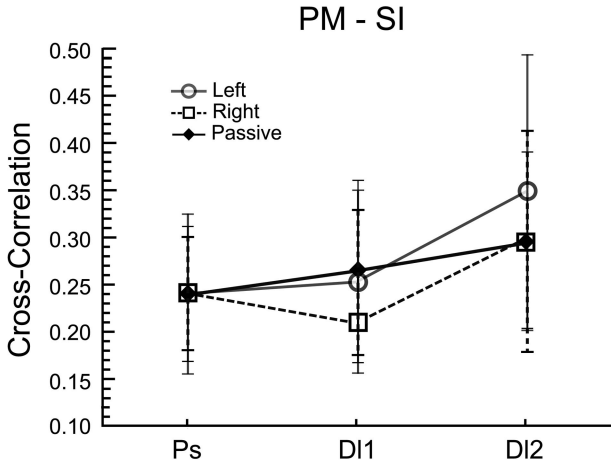

FIG. 10. Synchronization between the PM and SI LFPs, in the active condition left hand (open circles), the active condition right hand (open squares), and the passive condition (filled diamonds) in monkey F. Average and SD of cross-correlation coefficients calculated during the Ps, Dl1, and Dl2 delays for each condition, for the 10 sessions. Dl2 delay in the active left hand condition was the one that was the most different from the baseline Ps values.

hand, passive) × delay (3: Ps, Dl1, Dl2) MANOVA on the peak cross-correlation values for monkey F revealed a main effect of delay [$F(2,54) = 16.50$, $P < 0.0001$], but a delay × condition interaction that was not significant [$F(4,54) = 1.47$, $P = 0.223$]. Tukey's honest significant difference post hoc test showed that *1*) the delay Dl2 is different from the others and *2*) Dl2 of the left-hand active condition was the most different condition × time period element, from all the other Ps and Dl1 values. Monkey Z cross-correlations (recorded only during the active left hand and passive conditions) were also submitted to this analysis, revealing a main effect of delay [$F(2,8) = 5.20$, $P < 0.05$], but a condition × delay interaction that was not significant [$F(2,8) = 2.51$, $P = 0.142$]. Tukey's honest significant difference post hoc test showed that the delay Dl2 is different from the others, and that the left-hand active condition Dl2 TSE is different from the Dl1 TSE in the passive condition. For best PM–SI synchronization, the best task period was Dl2 of the left-hand active condition, during active waiting while the hand is resting on the lever just before the press. In addition, the right-hand active condition could be obstructing the difference between active and passive states: if the data from monkeys F and Z are grouped by considering only the left-hand active and passive conditions, the MANOVA provided a differential effect of these on the cross-correlation coefficients: a main effect of condition was found [$F(2,48) = 18.64$, $P < 0.0001$], as well as a condition × delay interaction [$F(2,48) = 4.21$, $P < 0.05$]. If only the left-hand active and passive conditions are considered, the task events produce a clear difference in the PM–SI cross-correlation coefficients: during Dl2, the left-hand condition requires a greater synchronization of the LFPs compared with the passive condition.

Factors affecting synchronization between the LFPs

Certain factors might explain the increase in synchronization during the active condition: with PM and SI showing strong oscillations during similar epochs, rhythmicity could act as a support for synchronization. Figure 11*A* shows the close relation between oscillatory 10- to 25-Hz content at the 2 sites with the cross-correlation coefficients at a given time. For this in-task data (one session, 79 trials), a 256-ms time window was moved every 128 ms, and the FFT % between 10 and 25 Hz, along with the cross-correlation coefficient, were computed for each window and each trial, and averaged across the trials. At high cross-correlation coefficient values (>0.42) the FFT % between 10 and 25 Hz was high for PM and SI. At lower cross-correlation coefficient values, the 10- to 25-Hz PM content was lower, whereas the SI content was just as high as for high cross-correlation coefficient values. SI LFPs can have high rhythmicity without the PM LFPs being as rhythmic, and that for high PM–SI synchronization, the PM has to become more rhythmic, possibly then driving the synchronization.

Another element was the lag between each LFP. A trial-by-trial analysis of the lag for one session (19 trials) was performed for 100 ms shifted 50 ms for precise identification of the mean and SD for each window. The results appear in Fig. 11*B*, and as in Fig. 9, prove that for the Dl2 period, not only did the lag approach zero, but also, when considering the variability, the SD decreased during that time period. LFPs became more synchronized as a result of a decreased variability of the lag just before the lever press.

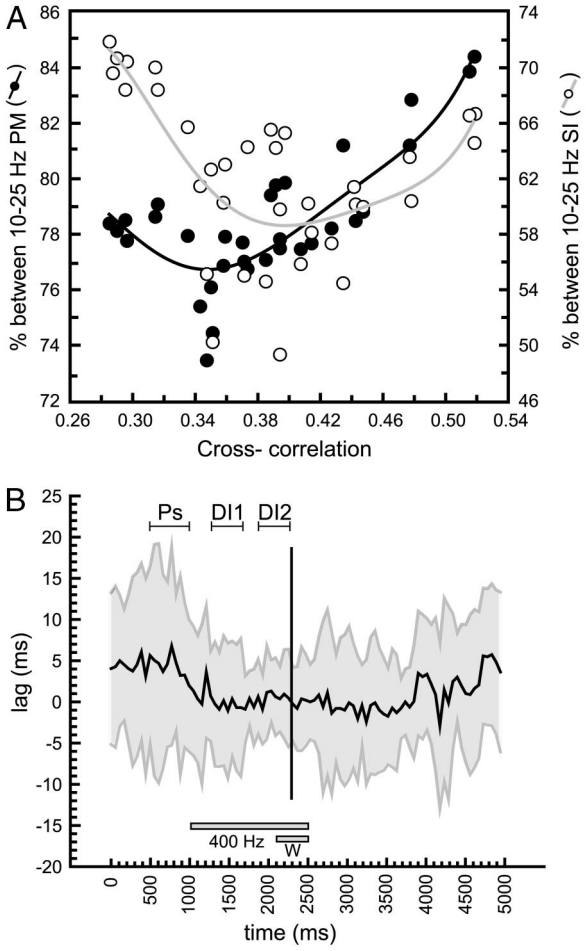

FIG. 11. Parameters affecting synchronization between PM and SI LFPs. *A*: relation between the cross-correlation coefficient (abscissa) and the oscillatory content at each LFP site (ordinate). *Left ordinate*: percentage of the LFP signal within 10–25 Hz at the PM site (black dots and line). *Right*: SI site (white dots, gray line). Values calculated on 36 windows of 256 ms shifted 128 ms, during the active condition, left hand. High cross-correlation values occurred when the 10- to 25-Hz oscillatory content was high at both the PM and SI sites. *B*: variability of the lag across the trial duration, calculated on a trial-by-trial basis for 19 trials during the active condition, left hand. Average, black line; ± SD, gray area; average time of lever press, vertical line. Sound stimulus (400 Hz) and reward window indicated at the *bottom*. For indicative purposes, the 3 delay windows are displayed: Ps (prestimulus), Dl1 (delay 1), Dl2 (delay 2).

Modulation and synchronization of PM and MI LFPs during active and passive expectancy

The modulation of the 10- to 25-Hz LFP oscillations in MI was similar to the one in SI (Fig. 12). Both PM and MI showed a similar pattern of modulation, where the initial stimulus-related decrease gave way to a return of the oscillations. Over many experiments, the modulation in the 10- to 25-Hz LFP MI oscillations was noticeable during the active task, and in 5 experiments where PM–MI recordings were performed, the decrease of the oscillations during Dl1 was again potent in both PM and MI (Fig. 12*B*). This pattern was true for the lever press with either hand. In the passive task, MI oscillations showed a different pattern, increasing during Dl1 and Dl2. A condition (3: active left hand, active right hand, passive) × area (2: PM,

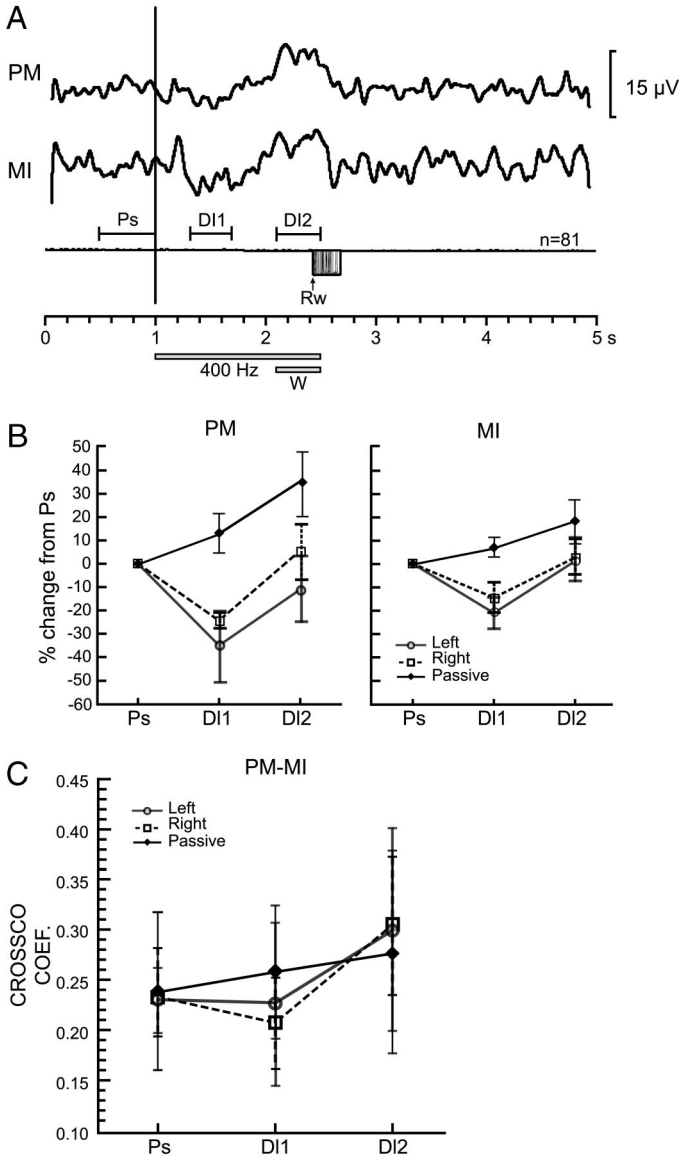

FIG. 12. Modulation and synchronization of PM and MI 10- to 25-Hz LFP oscillations during the active and passive conditions in monkey F. *A*: modulation of PM and MI 10- to 25-Hz oscillations during one experiment, active condition, left hand, as shown by the variations in the TSE throughout the trial duration. *Top 2 traces*: TSE values calculated from the 81 trials. *Bottom traces*: overlaid lever press contacts. Vertical line: onset of the 400-Hz sound stimulus, duration of which is shown by the rectangle labeled 400 Hz. W, reward window; Rw, reward. *B*: average ± 1SD of the relative TSE values for each condition during the Ps delay (fixed at 0% change) and the 2 other delays of interest, Dl1 and Dl2. On the left, PM sites; on the right, MI sites. *C*: synchronization between the PM and MI LFPs. For *B* and *C*, same symbols are used for the active condition left hand (open circles), the active condition right hand (open squares), and the passive condition (filled diamonds).

MI) × delay (2: Dl1, Dl2) MANOVA on the normalized TSE values for monkey F revealed a main effect of condition [$F(2,25) = 40.91$, $P < 0.0001$], of delay [$F(1,22) = 171.39$, $P < 0.0001$], interactions of condition by area [$F(2,22) = 4.75$, $P < 0.05$], and area × delay [$F(1,22) = 6.78$, $P < 0.05$]. Tukey's honest significant difference post hoc test showed that the PM passive condition Dl2 value was most different from that of all other condition × area × delays possibilities.

Figure 12*C* shows the PM–MI synchronization for the same experiments. A condition (3: active left hand, active right hand, passive) × delay (3: Ps, Dl1, Dl2) MANOVA on the cross-correlation coefficient values for monkey F revealed a main effect of delay [$F(2,22) = 8.89$, $P < 0.005$], but again a delay × condition interaction that was not significant [$F(4,22) = 0.97$, $P = 0.445$]. This lack of interaction could be attributable to the relatively small data set, or be indicative of PM–MI relations. Some experiments showed a high degree of synchronization, particularly in the left-hand active condition.

DISCUSSION

Simultaneous recordings of cerebral (particularly SI) and PM GCL LFP oscillations show similar 10- to 25-Hz oscillatory profiles and long-range synchronization between LFPs in the active condition. Compared with rest and prestimulus values, 10- to 25-Hz LFP oscillations became synchronized in the left-hand active condition, just before the lever press. Because of cerebro-cerebellar connectivity, the left-hand active condition is the most likely to show neural activity from the left PM and right SI to be simultaneously task-related. Synchronization during the task was clearly strongest in this condition, supporting a role for task-dependent synchronization during execution; nonetheless, it also increased slightly in the right-hand active and passive conditions, hinting a possible more general contribution in expectancy. Task-related modulations of the LFP oscillations in PM and cerebral cortex were condition-specific, but did not differentiate between left and right hands; synchronization was more sensitive to subtask specificities.

Independent but sometimes related oscillators in the cerebral cortex and cerebellum

The substrate producing the PM GCL oscillations has not been identified, contrary to the cerebral oscillations that are partly organized across the cortical layers and influenced by thalamic or reticular inputs (Lopes da Silva 1991; Munk et al. 1996; Steriade et al. 1990). However, LFP oscillations in the cerebellum are related to GCL multiunit activity (Courtemanche et al. 2002; Pellerin and Lamarre 1997), which could stem from granule cells, mossy fiber inputs, and/or inhibitory interneurons. GCL organization, through internal loops between granule cells and inhibitory interneurons, could explain the oscillatory phenomenon (Bell and Dow 1967; Maex and De Schutter 1998). Recordings from rat cerebellar cortex show that an inhibitory interneuron, the Lugaro cell, could fire rhythmically (6–20 Hz) under certain conditions (Holtzman et al. 2003). These local network properties of an intrinsic GCL rhythmogenesis could account for GCL LFP oscillations. These are not simply an afferent echo of oscillatory phenomena produced by the cerebral cortex, as the cross-correlation coefficient values between cerebral and cerebellar LFPs can be as low as around 0.2 (rest condition); cross-correlation coefficient values also vary across conditions. However, oscillators could functionally link, precisely what was studied here. Concerning the output, the GCL 10- to 25-Hz LFP oscillations are related to Purkinje cell simple spikes (Courtemanche et al. 2002), whereas interpositus nuclear cell activity also shows oscillatory activity (Aumann and Fetz 2002). The network dynamics remain elusive, although this oscillatory phenomenon seems to have far-reaching effects.

Oscillations and synchronization during the rest condition

Proportion of the LFP signal within 10–25 Hz at 2 remote sites such as PM and SI, or PM and MI, were linearly related during rest. In essence, strong 10- to 25-Hz oscillations at the cerebellar site were associated with strong oscillations at the cerebral cortex site. The PM–SI or PM–MI cross-correlations showed baseline levels around 0.2, similar to what we measured during the prestimulus delay during the active and passive conditions. Frequent zero-phase relations between the cerebellar and cerebral LFPs showed important timing properties of the synchronization. A narrow phase-advance for the MI versus PM LFPs could be dependent on the small data set, yet might mean that MI leads the influence to the PM. In any case, measurements during rest provided baseline values for oscillations and synchronization, yet these showed variability, possibly indicative of the animal's freedom to adopt various internal states, out-of-task.

Paramedian lobule—somatosensory cortex LFP relations

PM LFP oscillations are differentially modulated during active and passive expectancy (Courtemanche et al. 2002). During active expectancy, these oscillations showed a poststimulus decrease, a return to Ps values before lever press, and a subsequent decrease; this differed from passive expectancy, where the stimulus triggered an increase in oscillations lasting until the reward. Here, in PM–SI recordings, SI LFP oscillations showed the same decrease–return–decrease pattern during the active condition. Increased 20- to 25-Hz oscillations in areas 5 and 7 also occur during movement preparation (MacKay and Mendonça 1995). SI oscillations gradually increased during reward expectancy in the passive condition, in a pattern similar to heightened mu-band oscillatory activity during expectancy without movement (Rougeul et al. 1979). The right-hand active condition and the passive condition produced a moderate increase in the synchronization from Ps values, but the left-hand active condition showed the clearest examples of increased synchronization. This condition- and limb-specific increase in synchronization points to a more subtle role for synchronization versus strength of oscillation in network relations. The left-hand active condition produced the best increase in both the oscillatory profile and the PM–SI synchronization before the lever press.

There is a strong PM–SI connection: the PM GCL receives input from the parietal cortex through the lateral pontine nuclei and the lateral reticular nucleus (Allen and Tsukahara 1974; Bloedel and Courville 1981), a possible substrate for the synchronization seen here. Electrophysiological mapping offers evidence that the parietal cortex is preferentially connected with the posterior lobe of the cat cerebellum (Sasaki et al. 1975); in monkeys, still part of the PM afferents come originally from the parietal cortex (Sasaki 1979). Corticopontine projections arising from areas 1 and 2 are substantial (Vassbo et al. 1999), and inputs from the contralateral pontocerebellar fibers are the most numerous to the PM (King et al. 1998). These terminate more in the apex of the lobule (Voogd and Glickstein 1998), which corresponds to the location of the cerebellar PM 10- to 25-Hz LFP oscillations.

The cerebellum also receives from the cerebral cortex by the lateral reticular nucleus (Clendenin et al. 1974), which may influence synchronization: the lateral reticular nucleus neurons offer rhythmic discharges in the 10- to 25-Hz range (J.-P. Pellerin, R. Courtemanche and Y. Lamarre, unpublished observations). However, cortico-ponto-cerebellar connections are far more numerous, and could subserve an important cerebro-cerebellar remapping: a 10- to 50-Hz cerebro-pontine paired-pulse stimulation pattern provides the highest EPSPs in pontine cells (Schwarz and Thier 1999). Because of the zero phase lag, perhaps a third site, such as the thalamus or the basal ganglia, could influence the synchronization. Cerebellothalamic connections to the ventrolateral nucleus modulate somatosensory information going to the forebrain (Crispino and Bullock 1984), and cerebellar output through this pathway could affect epileptic seizures (Kandel and Buzsáki 1993). Thalamocortical oscillations during sleep are influenced by cerebellar output, as Timofeev and Steriade (1997) showed that the cerebellothalamic pathway exhibits 30- to 100-Hz oscillations that become synchronized with cortical oscillations. During movement, magnetoencephalographic measurements (Gross et al. 2002) show that cerebello-thalamo-cortical sites synchronize their 6- to 9-Hz oscillatory activity, showing a phase advance for the cerebellum (cerebellum–thalamus–MI–SI–cerebellum sequence). Although we did see a timing difference between LFPs during rest (MI before PM, PM before SI), this difference was not evident during active expectancy, with the PM initially leading SI, but as premovement immobility occurs, the lag falls to zero. The difference could be related to a variety of factors (species-related, methodology-related, or even possibly rhythm-specific).

Overall, these anatomical and electrophysiological studies provide evidence for a strong connection between PM and SI, probably at the source of the synchronization. Although the GCL oscillations could still partly stem from cerebral oscillations, synchronization was weaker for the passive condition during Dl2 even with strong oscillations: this precludes a simple direct transmission, probably as modulation occurs at the pontine level, through various ponto-cerebellar loops (Schwarz and Thier 1999).

Paramedian lobule–motor cortex LFP relations

PM–MI relations were different between the active and passive conditions. Although probably from different generators, SI and MI LFPs can show similar patterns of oscillation in motor tasks (Murthy and Fetz 1996). However, whereas MI oscillations showed a less profound modulation than PM oscillations during the active condition, the most important difference concerned the PM–MI synchronization, which did not differentiate between the left and right hands, both showing a similar pattern relative to the lever press. The PM–MI synchronization thus seemed less limb-specific than the PM–SI synchronization. Others also found for MI LFP oscillations a similar nonspecificity with movement parameters, within a closely related frequency band (Donoghue et al. 1998; Murthy and Fetz 1996), yet this could be different for higher bands. The sensitivity of LFP modulation to task parameters could be band-specific and better in higher bands, as for parietal recordings (Pesaran et al. 2002).

Possible functions of LFP oscillations and synchronization in cerebro-cerebellar relations

Intentionally, we omitted labeling the synchronization as "cerebro-cerebellar" because the recorded sites were not proven to communicate directly, by verification of specific site-to-site connections. However, the PM–SI receptive fields were partially overlapping because SI receptive fields were on the contralateral arm and the PM receptive fields often spanned more than one limb, including the receptive fields for SI. The MI sites were part of an excitable zone of cortex at currents of <10 μA, triggering movement of the contralateral proximal musculature. To discuss our results as cerebro-cerebellar, sites should be proven connected: however, the present study probably includes LFP recording sites that would be part of such a precisely defined sample of sites.

We show here a heightened synchronization preferentially between oscillating LFPs recorded in the PM and SI versus PM and MI, during the active task, and also preferentially for the related hand. Rhythm modulation was not hand specific, but differentiated between active and passive conditions. The simultaneous breakdown of the oscillations in PM, SI, and MI after the stimulus, the subsequent return, and the decrease again after the lever press is reminiscent of the modulation shown for SI and MI during active expectancy (Donoghue et al. 1998; MacKay and Mendonça 1995; Murthy and Fetz 1996; Rougeul et al. 1979), and compares with modulation of striatal oscillations (Courtemanche et al. 2003). However, SI and MI oscillatory modulation during the passive condition is more progressive and oscillations increase in amplitude: this could indicate a mechanism to evaluate delays, and optimize local circuits, possibly by a process resembling attention (Lebedev and Wise 2000; Pfurtscheller 1981; Rougeul et al. 1979). However, synchronization of cerebral and cerebellar oscillations was stronger in the active condition, and more sensitive to the subtask elements, such as the hand used for the task.

In the rat, such higher synchronization (coherence) appears between vibrissa area SI and Crus LFPs, particularly for the 6- to 10-Hz and 15- to 19-Hz bands during whisking, but also occurred when the animal was immobile (O'Connor et al. 2002). These 2 frequencies could be part of an internal reverberating state (Hartmann and Bower 1998), favoring SI–Crus communication during periods of whisking because the pause states were temporally close to the whisking episodes. Increased rhythmicity during the active condition left-hand task could represent a somatosensory reverberation mechanism to help cerebro-cerebellar communication PM–SI synchronization. At the same time, the strength of the PM–SI synchronization during the left-hand active condition, along with the frequent overlap of somatosensory receptive fields between PM and SI, point to a possible somatosensory processing role for the synchronization. Precisely, the exact timing of the PM–SI synchronization increase, during Dl2, as the hand was resting on the lever in preparation for the press (see Fig. 9 for the strain gauge signal), provide support for a PM–SI collaboration in the processing of the somatosensory input to the hand. The contribution could be distinct within each area, with the clear tactile component being processed in the SI local circuits, and possibly the optimization of the sensory input being evaluated in the PM local circuits (Bower 1997). Somatosensory cortex and the posterior lobe of the cerebellum communicate with the express goal of sharing information about sensory input (Bower and Kassel 1990; Morissette and Bower 1996; O'Connor et al. 2002). In our study, the increased synchronization was seen only for the anatomically linked hand, and was strongest when the animal was lightly touching the lever, waiting for the proper time to press; at that precise instant, SI circuits are perhaps evaluating the level of pressure to be maintained for the timely release of the lever, and PM circuits could in turn be optimizing the orientation of the sensory surfaces for the best available information about the pressure. The LFP synchronization could be supporting the communication between the 2 areas, which it seems bases itself on the reverberating local signals within PM and SI. The cerebellar GCL is strongly influenced by tactile stimulation: in measuring GCL multiunit activity in the Crus of awake behaving rodents, Hartmann and Bower (2001) found GCL activity to correlate directly with exploratory tactile stimulation of orofacial receptive fields during active exploration, and Golgi cells also show a well-structured response to somatosensory stimulation (Vos et al. 1999). For a more complete evaluation of the possibility that the increased synchronization is purely related to somatosensory processing, more complete testing would require precise measurements of SI and GCL unit activity, along with a better control of the somatosensory stimulus, which fell outside the scope of the current study.

In comparison, increased oscillations during the passive condition without increased synchronization throughout PM, SI, and MI also point to the independence of the reverberation process with the synchronization. During reward expectation, oscillations increased in all 3 areas, possibly preparing circuits for optimal analysis of information. In cases when interareal communication occurs, oscillations would facilitate synchronization during performance, serving to gather information (MacKay 1997). Both the parietal cortex and cerebellum contribute to the shifting of attention (Courchesne et al. 1994; Huu Le et al. 1998): oscillations in both could indicate a "readiness" of the system, with synchronization serving for exchange of information.

ACKNOWLEDGMENTS

The authors thank M.-T. Parent for excellent technical work throughout the project; M. Yeates for figure preparation; C. Valiquette and G. Richard for computer programming and hardware; and T. Drew, E. Chapman, A. Smith, and J.-P. Pellerin for technical help and discussions.

GRANTS

This work was supported by a group grant from the Canadian Institutes of Health Research, and by grants from the Fonds pour les Chercheurs et l'Aide à la Recherche, Québec, and National Alliance for Autism Research to Y. Lamarre. R. Courtemanche received scholarship support from the Natural Sciences and Engineering Research Council and Fonds de la Recherche en Santé-FCAR-Santé. Final steps were performed as R. Courtemanche received a Concordia University General Research Funds grant.

REFERENCES

Allen GI and Tsukahara N. Cerebrocerebellar communication systems. *Physiol Rev* 54: 957–1006, 1974.

Aumann TD and Fetz EE. Oscillatory activity in cerebellar nuclei of primates performing limb movements. *Soc Neurosci Abstr* 28: 360.7, 2002.

Baker SN, Olivier E, and Lemon RN. Coherent oscillations in monkey motor cortex and hand muscle EMG show task-dependent modulation. *J Physiol* 501: 225–241, 1997.

Bell CC and Dow RS. Cerebellar circuitry. *Neurosci Res Prog Bull* 5: 121–222, 1967.

Bloedel JR and Courville J. Cerebellar afferent systems. In: *Handbook of Physiology. The Nervous System. Motor Control*. Bethesda, MD: Am. Physiol. Soc., 1981, sect. 1, vol. II, pt. 2, p. 735–829.

Bower JM. Control of sensory data acquisition. In: *The Cerebellum and Cognition* (International Review of Neurobiology series), edited by Schmahmann JD. San Diego, CA: Academic Press, 1997, vol. 41, p. 489–513.

Bower JM and Kassel J. Variability in tactile projection patterns to cerebellar folia Crus IIA of the Norway rat. *J Comp Neurol* 302: 768–778, 1990.

Classen J, Gerloff C, Honda M, and Hallett M. Integrative visuomotor behavior is associated with interregionally coherent oscillations in the human brain. *J Neurophysiol* 79: 1567–1573, 1998.

Clendenin M, Ekerot C-F, Oscarsson O, and Rosén I. The lateral reticular nucleus in the cat. I. Mossy fibre distribution in cerebellar cortex. *Exp Brain Res* 21: 473–486, 1974.

Courchesne E, Townsend J, Akshoomoff NA, Saitoh O, Yeung-Courchesne R, Lincoln AJ, James HE, Haas RH, Schreibman L, and Lau L. Impairment in shifting attention in autistic and cerebellar patients. *Behav Neurosci* 108: 848–865, 1994.

Courtemanche R, Fujii N, and Graybiel AM. Synchronous, focally modulated beta-band oscillations characterize local field potential activity in the striatum of awake behaving monkeys. *J Neurosci* 23: 11741–11752, 2003.

Courtemanche R and Lamarre Y. Localization of cerebellar oscillatory activity of the awake monkey and relation with cortical rhythms. *Soc Neurosci Abstr* 23: 1286, 1997.

Courtemanche R, Parent M-T, and Lamarre Y. Cerebro-cerebellar and intracerebellar synchronization of local field potential oscillations in the monkey performing a behavioral task. *Soc Neurosci Abstr* 25: 373, 1999.

Courtemanche R, Pellerin J-P, and Lamarre Y. Local field potential oscillations in primate cerebellar cortex: modulation during active and passive expectancy. *J Neurophysiol* 88: 771–782, 2002.

Crispino L and Bullock TH. Cerebellum mediates modality-specific modulation of sensory responses of midbrain and forebrain in rat. *Proc Natl Acad Sci USA* 81: 2917–2920, 1984.

Csicsvari J, Henze DA, Jamieson B, Harris KD, Sirota A, Bartho P, Wise KD, and Buzsaki G. Massively parallel recording of unit and local field potentials with silicon-based electrodes. *J Neurophysiol* 90: 1314–1323, 2003.

Donoghue JP, Sanes JN, Hatsopoulos NG, and Gaál G. Neural discharge and local field potential oscillations in primate motor cortex during voluntary movement. *J Neurophysiol* 79: 159–173, 1998.

Feige B, Aertsen A, and Kristeva-Feige R. Dynamic synchronization between multiple cortical motor areas and muscle activity in phasic voluntary movements. *J Neurophysiol* 84: 2622–2629, 2000.

Gross J, Timmermann L, Kujala J, Dirks M, Schmitz F, Salmelin R, and Schnitzler A. The neural basis of intermittent motor control in humans. *Proc Natl Acad Sci USA* 99: 2299–2302, 2002.

Hartmann MJ and Bower JM. Oscillatory activity in the cerebellar hemispheres of unrestrained rats. *J Neurophysiol* 80: 1598–1604, 1998.

Hartmann MJ and Bower JM. Tactile responses in the granule cell layer of cerebellar folium crus IIa of freely behaving rats. *J Neurosci* 21: 3549–3563, 2001.

Holtzman T, Phuah C, and Edgley S. Oscillatory spike trains in the cerebellar cortex; a possible connection with Lugaro cells? *Soc Neurosci Abstr* 33: 75.7, 2003.

Huu Le T, Pardo JV, and Hu X. 4 T-fMRI study of nonspatial shifting of selective attention: cerebellar and parietal contributions. *J Neurophysiol* 79: 1535–1548, 1998.

Kandel A and Buzsáki G. Cerebellar neuronal activity correlates with spike and wave EEG patterns in the rat. *Epilepsy Res* 16: 1–9, 1993.

King VM, Armstrong DM, Apps R, and Trott JR. Numerical aspects of pontine, lateral reticular, and inferior olivary projections to two paravermal cortical zones of the cat cerebellum. *J Comp Neurol* 390: 537–551, 1998.

König P and Engel AK. Correlated firing in sensory-motor systems. *Curr Opin Neurobiol* 5: 511–519, 1995.

Lamarre Y, Joffroy AJ, Filion M, and Bouchoux R. A stereotaxic method for repeated sessions of central unit recording in the paralyzed or moving animal. *Rev Can Biol* 29: 371–376, 1970.

Lebedev MA and Wise SP. Oscillations in the premotor cortex: single unit activity from awake, behaving monkeys. *Exp Brain Res* 130: 195–215, 2000.

Liang H, Bressler SL, Ding M, Truccolo WA, and Nakamura R. Synchronized activity in prefrontal cortex during anticipation of visuomotor processing. *Neuroreport* 13: 2011–2015, 2002.

Lopes da Silva FH. Neural mechanisms underlying brain waves: from neural membranes to networks. *Electroencephalogr Clin Neurophysiol* 79: 81–93, 1991.

MacKay WA. Synchronized neuronal oscillations and their role in motor processes. *Trends Cogn Sci* 1: 176–183, 1997.

MacKay WA and Mendonça AJ. Field potential oscillatory bursts in parietal cortex before and during reach. *Brain Res* 704: 167–174, 1995.

Maex R and De Schutter E. Synchronization of Golgi and granule cell firing in a detailed network model of the cerebellar granule cell layer. *J Neurophysiol* 80: 2521–2537, 1998.

Marsden JF, Werhahn KJ, Ashby P, Rothwell J, Noachtar S, and Brown P. Organization of cortical activities related to movement in humans. *J Neurosci* 20: 2307–2314, 2000.

Mehring C, Rickert J, Vaadia E, Cardoso de Oliveira S, Aertsen A, and Rotter S. Inference of hand movements from local field potentials in monkey motor cortex. *Nat Neurosci* 6: 1253–1254, 2003.

Morissette J and Bower JM. Contribution of somatosensory cortex to responses in the rat cerebellar granule cell layer following peripheral tactile stimulation. *Exp Brain Res* 109: 240–250, 1996.

Munk MHJ, Roelfsema PR, König P, Engel AK, and Singer W. Role of reticular activation in the modulation of intracortical synchronization. *Science* 272: 271–274, 1996.

Murthy V and Fetz EE. Oscillatory activity in sensorimotor cortex of awake monkeys: synchronization of local field potentials and relation to behavior. *J Neurophysiol* 76: 3949–3967, 1996.

O'Connor S, Berg RW, and Kleinfeld D. Coherent electrical activity between vibrissa sensory areas of cerebellum and neocortex is enhanced during free whisking. *J Neurophysiol* 87: 2137–2148, 2002.

Pellerin J-P and Lamarre Y. Local field potential oscillations in primate cerebellar cortex during voluntary movement. *J Neurophysiol* 78: 3502–3507, 1997.

Pesaran B. Using local field potentials for a brain–computer interface. *Soc Neurosci Abstr* 33: 650.3, 2003.

Pesaran B, Pezaris JS, Sahani M, Mitra PP, and Andersen RA. Temporal structure in neuronal activity during working memory in macaque parietal cortex. *Nat Neurosci* 5: 805–811, 2002.

Pfurtscheller G. Central beta rhythm during sensorimotor activities in man. *Electroencephalogr Clin Neurophysiol* 51: 253–264, 1981.

Roelfsema PR, Engel AK, König P, and Singer W. Visuomotor integration is associated with zero time-lag synchronization among cortical areas. *Nature* 385: 157–161, 1997.

Rougeul A, Bouyer JJ, Dedet L, and Debray O. Fast somato-parietal rhythms during combined focal attention and immobility in baboon and squirrel monkey. *Electroencephalogr Clin Neurophysiol* 46: 310–319, 1979.

Salmelin R and Hari R. Spatiotemporal characteristics of sensorimotor neuromagnetic rhythms related to thumb movement. *Neuroscience* 60: 537–550, 1994.

Sasaki K. Cerebro–cerebellar interconnections in cats and monkeys. In: *Cerebro–Cerebellar Interactions*, edited by Massion J and Sasaki K. Amsterdam: Elsevier/North-Holland Biomedical Press, 1979, p. 105–124.

Sasaki K, Oka H, Matsuda Y, Shimono T, and Mizuno N. Electrophysiological studies of the projections from the parietal association area to the cerebellar cortex. *Exp Brain Res* 23: 91–102, 1975.

Schwarz C and Thier P. Binding of signals relevant for action: towards a hypothesis of the functional role of the pontine nuclei. *Trends Neurosci* 22: 443–451, 1999.

Steriade M, Gloor P, Llinás RR, Lopes da Silva FH, and Mesulam MM. Basic mechanisms of cerebral rhythmic activities. *Electroencephalogr Clin Neurophysiol* 76: 481–508, 1990.

Timofeev I and Steriade M. Fast (mainly 30–100 Hz) oscillations in the cat cerebellothalamic pathway and their synchronization with cortical potentials. *J Physiol* 504: 153–168, 1997.

Vassbo K, Nicotra G, Wiberg M, and Bjaalie JG. Monkey somatosensory cerebrocerebellar pathways: uneven densities of corticopontine neurons in different body representations of areas 3b, 1, and 2. *J Comp Neurol* 406: 109–128, 1999.

Voogd J and Glickstein M. The anatomy of the cerebellum. *Trends Neurosci* 21: 370–375, 1998.

Vos BP, Volny-Luraghi A, and De Schutter E. Cerebellar Golgi cells in the rat: receptive fields and timing of responses to facial stimulation. *Eur J Neurosci* 11: 2621–2634, 1999.